MICROSTRUCTURE AND PROPERTIES OF LASER DEPOSITED AND WROUGHT ALLOY K-500 (UNS N05500)

P.W. Hochanadel, R.D. Field and G.K. Lewis

ABSTRACT

Feasibility tests were performed by manufacturing transition joints between Nickel-200 (Ni-200) and Alloy K-500 (K-500) with direct laser deposition. Both sharp and functionally graded interfaces were manufactured with no apparent issues. In addition, Alloy K-500 specimens were manufactured with direct laser deposition to analyze the isothermal hardening response of Alloy K-500. The laser deposited and wrought materials were precipitation hardened at three different temperatures (600 °C, 650 °C, and 700 °C) and various times. A relationship between the hardness and the volume fraction of $Ni_3(Ti,Al)$ was developed, and the subsequent analysis showed that the corresponding Johnson-Mehl-Avrami time constants (or n-values) ranged from 1.1 to 1.3 at an aging temperature 600 °C, and decreased to values ranging from 0.6 to 0.66 at an aging temperature of 700 °C. For site saturation and spherical precipitates, the expected n-value is 1.5. This analysis showed that the mechanism for precipitation changed as a function of temperature. The results of the analysis at higher temperatures were rationalized by the possibility of the decay of quenched-in vacancies, precipitation along the grain boundaries, and precipitation along the dislocations. It was, however, difficult to confirm these possibilities with transmission electron microscopy (TEM), since imaging the precipites is difficult at very early aging times. Finally, it was determined that the heat treatment schedule of laser welded or laser clad Alloy K-500 should be similar to that of wrought Alloy K-500.

IIW-Thesaurus keywords: Deposition; Dissimilar; Metals; Laser, Metallurgy, Nickel Alloys.

1 Introduction

Direct laser deposition is a process that is able to build transition joints for dissimilar welding applications, in which the careful control of the chemical composition is needed or desired. Directed Light Fabrication (DLF) is a direct laser fabrication technique in which metal powder is placed at the focal point of a laser with sufficient power to melt the powder. This is essentially a multi-pass laser welding/cladding process in which filler metal (as powder) is utilized. By designing and controlling the movement of the laser with a computer, a controlled amount of cladding may be applied to the surface of a substrate or a solid, three-dimensional part can be built.

Alloy K-500 (K-500) is a nickel-copper alloy which is similar to Alloy 400 (approximately 65 weight percent nickel and 30 weight percent copper), but containing alloying additions of approximately 2-3 weight percent aluminum and approximately one-half weight percent titanium for added strength. In K-500, precipitation of $Ni_3(Ti, Al)$ gamma-prime ($L1_2$) occurring throughout the fcc, Ni-Cu matrix allows for added strength. Besides its higher potential strength, alloy K-500 has good corrosion resistance in a variety of environments, such as acid, alkali, salt water and sour-gas (hydrogen sulfide). This alloy is particularly attractive in chemical, marine and oil/gas applications such as valves, marine fittings, pump shafts and impellers, oil well drill collars and condensor tubing in heat exchangers. In addition, this alloy has found aerospace applications such as the oxygen recharger compressor assemblies in the International Space Station.

To date, the precipitation behavior of wrought K-500 has been investigated by Dey and Mukhopadhyay [1] and Dey *et al.* [2]. They characterized the precipitation behavior in terms of morphology and distribution. The kinetics of precipitation were modeled based upon theoretical strengthening laws. Insufficient data were presented to model the early times in aging (*i.e.*, prior to the peak strength), and were not investigated in terms of overall transformation kinetic theory, which would allow for the prediction of precipitation in terms of nucleation and growth theories prior to overaging. Rather, the data were analyzed purely in terms of strengthening models to predict strength as a function of precipitate diameter. To date, no studies have been performed on the precipitation kinetics of gamma-prime precipitation in laser welded alloy K-500.

This study was performed to investigate the feasibility of producing transition metal joints between materials (with

IIW-2279, recommended for publication by Commission IV "Power Beam Processes."

both sharp and functionally graded interfaces) by utilizing both Nickel-200 (Ni-200) and K-500. Further, this study was undertaken to investigate the precipitation kinetics of gamma-prime in both direct laser deposited and wrought K-500 utilizing overall transformation kinetic models. The ultimate reason for analyzing the kinetics of nucleation and growth of precipitates in DLF/laser welded material is to be able heat treat components after direct laser manufacturing or laser welding/cladding with known parameters and predict the hardness or strength in the weld/graded areas.

2 Experimental procedure

Alloy K-500 was obtained in the form of 127-mm (5-in.) diameter bar stock. Also, K-500 powder was obtained for the laser deposition. The composition ranges of both materials appear in Table 1. It should be noted that the powder K-500 contained 0.52 weight percent Ti compared to 0.48 weight percent Ti in the wrought. Similarly, the powder K-500 contained 2.69 weight percent Al compared to 3.02 weight percent Al in the wrought material. This is important to note, since these elements are primary elements in the strengthening precipitates – Ni_3(Ti, Al). The wrought material was cross-sectioned to provide 127-mm diameter by approximately 6 mm-thick plates. The laser deposited samples were fabricated by using the directed light fabrication (DLF) system at Los Alamos; the fabrication parameters are provided in Table 2. The specimen size for hardness coupons was approximately 5 mm × 10 mm × 110 mm. Feasibility coupons for transition metal joints were made by utilizing Ni-200 plate, Ni-200 powder and K-500 powder.

Heat treatments for the isothermal precipitation kinetics investigation were carried out in two steps: (1) solution heat treating at 1000 °C for 1 hour and (2) aging at temperatures of 600 °C, 650 °C or 700 °C for times varying between 30 seconds and 4 days. Solution heat treating and longer aging treatments were both performed in a standard non-vacuum furnace and water-quenched. Oxide scale was removed by carefully grinding. Shorter time heat treatments were performed in a Gleeble 1500/20 thermomechanical simulator to insure specimen temperature and allow for rapid heating and cooling, all while in a controlled atmosphere (vacuum atmosphere of 8×10^{-4} torr or lower). The feasibility coupons were solution heat treated at 1000 °C and then aged for 8 hours at 650 °C. Samples were then hardness tested (both Rockwell and microhardness testing). Light microscopy and transmission electron microscopy (TEM) was used to characterize the microstructures. Specimens for microscopy were prepared by standard metallographic procedures.

3 Results

Cross-sections of the feasibility coupons are given in Figures 1 a) and 1 b). Both the sharp interface [Figure 1 a)] and the functionally graded interface [Figure 1 b)] for the transition joints between Ni-200 and K-500 are presented. The microhardness profiles for the sharp interface and the functionally graded interface are given in Figures 1 c) and 1 d), respectively. In addition, the mass percent copper appears on the same plot to illustrate the composition change as a function of position in both sharp and functionally graded interfaces. Both the microhardness and the amount of copper were found to decrease rapidly at the K-500/Ni-200 interface, as expected. Specifically, the mass percent copper was observed to change from 30 % (on the K-500 side) to 0 % (on the Ni-200 side). The Ni-200 was plate material in this case. In the specimen that contained a functionally graded interface, both the Ni-200 and K-500 were deposited, and the dilution of copper in the Ni-200 material was similar, but the material was graded gradually from 30 % to 0 % copper by mass.

The hardness data for the isothermal precipitation kinetics analysis appear in Figure 2. As illustrated in this figure, the as-DLF material was found to harden rapidly, especially at 700 °C. All three materials (wrought and solution annealed, DLF and solution annealed and as-DLF)

Table 1 – Chemical Composition Ranges for Ni-200 and K-500 (in Weight Percent) of the Materials Investigated (maximum values indicated unless otherwise noted)

	C	Mn	Fe	S	Si	Cu	Ni	Al	Ti	Other
Ni-200	0.15	0.35	0.4	0.01	0.35	0.25	99.0 min	n/a	n/a	Mn - 0.35
K-500 (nom.)	0.25	1.50	2.0	0.01	0.50	27.00-33.00	See other	2.30-3.15	0.35-0.85	+Co – 63.0 min

Table 2 – Laser Deposition Parameters

Laser Power	350 W
Powder Feed Rate	0.12 g/s (average)
Powder Size	45-105 µm
Traverse Speed	17 mm/s

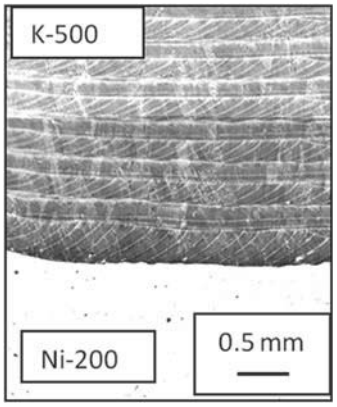

a)

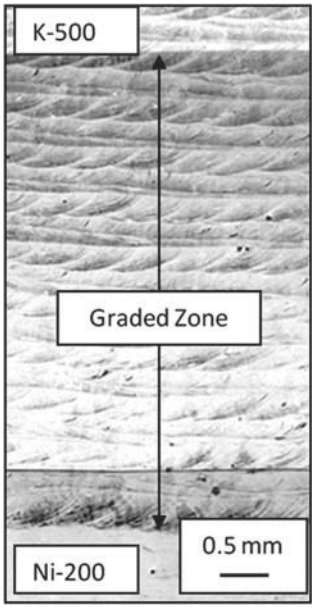

b)

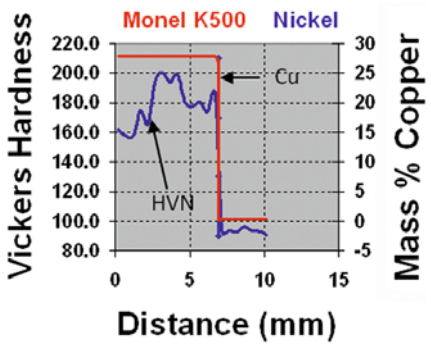

c)

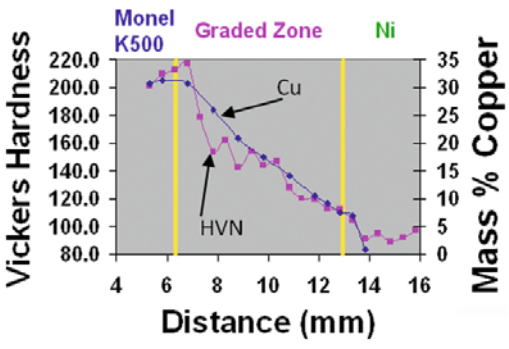

d)

Figure 1 – Light micrographs of sharp interface a) and graded interface of Nickel 200 and K-500 b). The corresponding microhardness and weight percent copper for the sharp interface c) and graded interface d) are shown for comparison

exhibited similar behavior. This is illustrated in Figure 3, in which the hardening behavior of all three of the materials at 600 °C is seen. The hardness/time/temperature behavior was found to be similar to that of Dey *et al.* [2], but slightly more rapid. However, Dey *et al.* [2] did not investigate the early time precipitation kinetics presented

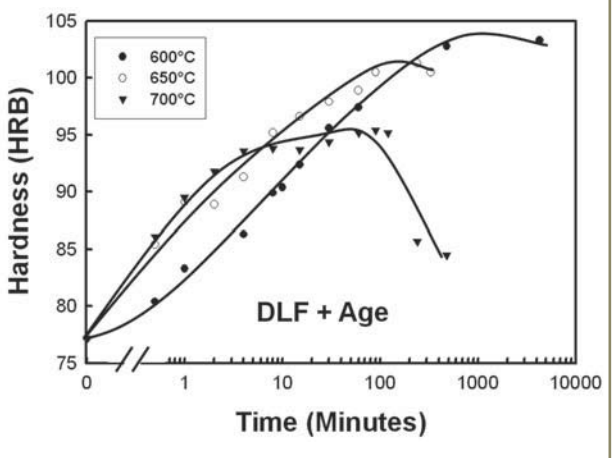

Figure 2 – Isothermal hardening kinetics curves at various temperatures for the laser-deposited alloy K-500

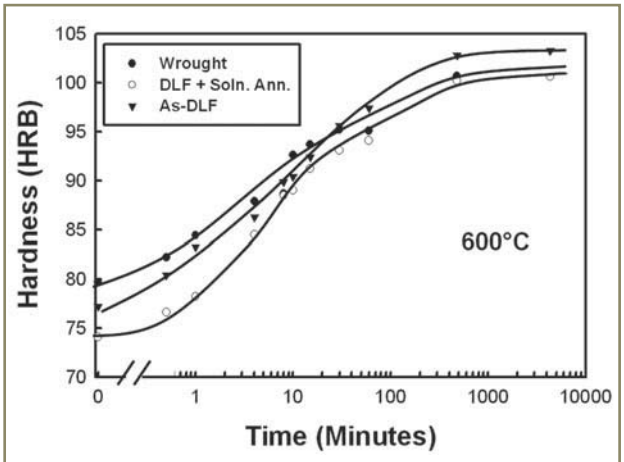

Figure 3 – Isothermal analysis of the hardening kinetics in alloy K-500. Wrought, DLF and solution annealed (DLF + Soln. Ann) and as-DLF are shown for comparison

in the present investigation. The wrought material was found to harden slightly more rapidly than either of the DLF materials, and did not harden to the extent of the direct fabricated materials.

The microstructure of the as-DLF material is seen in Figure 4. This material was observed to have a microstructure similar to laser welded materials (*i.e.,* a fine cellular microstructure typically observed in fcc weld metal, such as austenitic stainless steel like type 304L stainless steel [3]). The microstructure was found to be cellular/cellular dendritic with cell spacing on the order of 10 μm.

The as-DLF alloy material did not exhibit a high dislocation density and only slight evidence of precipitation was observed, as seen in the transmission electron results of Figure 5. Figure 5 a) shows the TEM bright field micrograph for the as-DLF alloy K-500, while Figure 5 b) presents the corresponding electron diffraction pattern. Note that very faint superlattice reflections may be observed in Figure 5 b), indicating that a very small amount of $Ni_3(Ti, Al)$ has already precipitated, which is not discernable in the bright field TEM.

DLF material aged at 650 °C for 8 hours (slightly overaged) was observed to have substantial gamma-prime precipitation. Figure 6 presents the dark field TEM micrograph and corresponding electron diffraction pattern for this material. Note that, even after the peak hardness is realized, the gamma-prime precipitation remains spherical, which is similar to the results obtained by Dey *et al.* [2]. Also, the distribution of gamma-prime precipitates appears to be mostly uniform, with a small amount along grain boundaries and dislocations. These were found to be slightly larger than those found randomly in the matrix. Although not presented here, elongated precipitates were found trailing a migrating grain boundary in the slightly overaged K-500. These observations were similar to those of Dey and Mukhophadhyay [1] and Dey *et al.* [2].

4 Model

Early in aging, (*i.e.*, typically a small radius and lower volume fraction of precipitate), the strengthening of K-500

a)

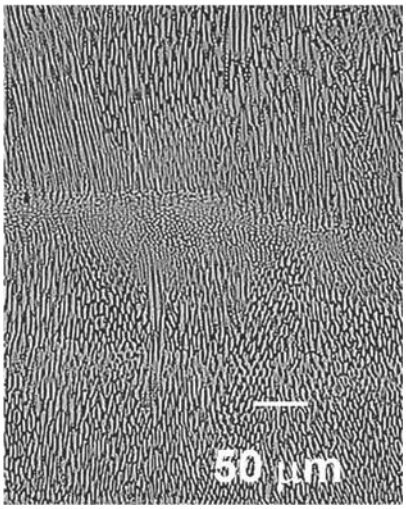

b)

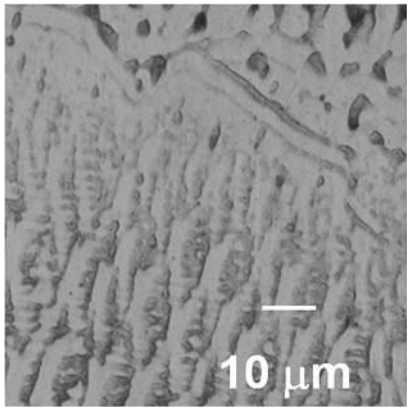

c)

Figure 4 – Light micrographs of as-DLF alloy K-500. The lower magnification view is seen in a), and progressively higher magnification is seen in b) and c)

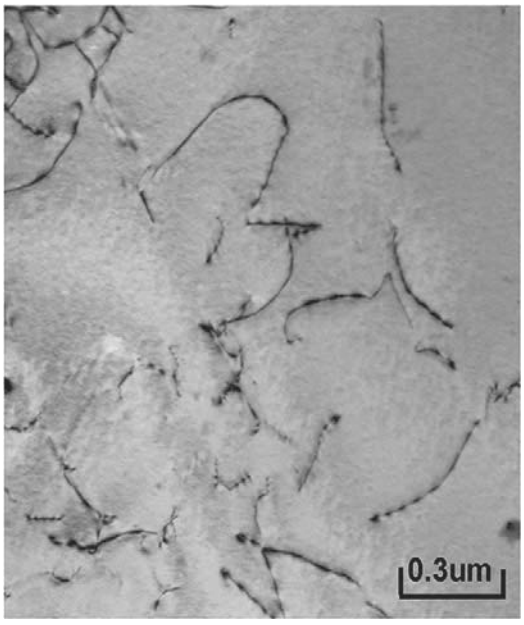

a)

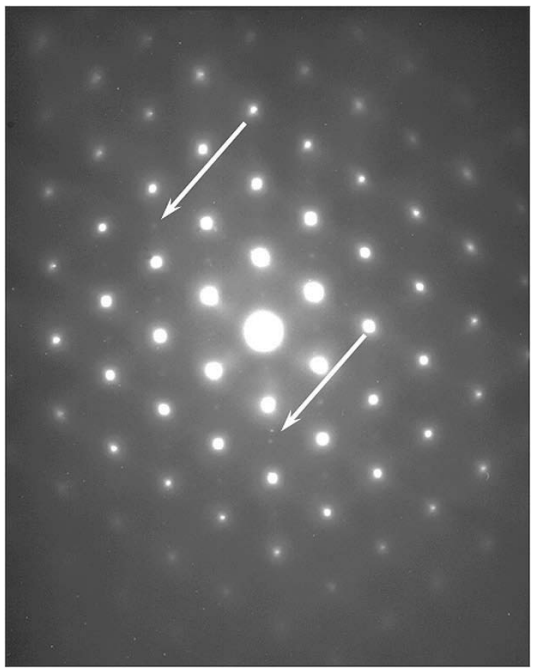

b)

Figure 5 – Transmission electron micrograph of as-DLF alloy K-500. The bright field is seen in a) and the corresponding electron diffraction pattern is seen in b). Note very faint superlattice reflections in (b) indicating a small amount of precipitation has occurred

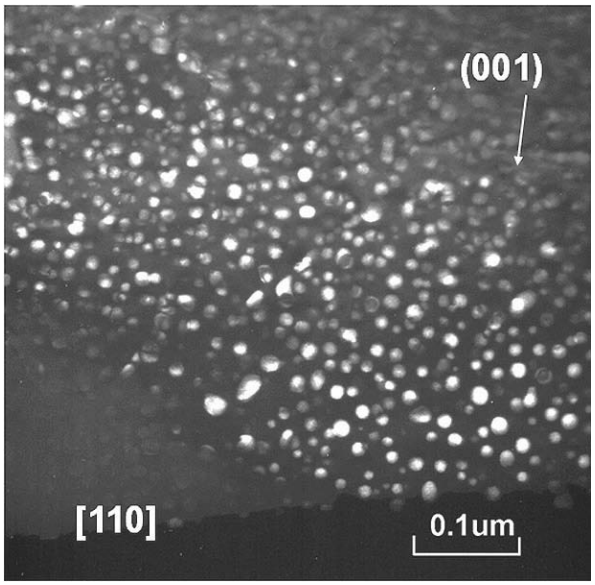

a)

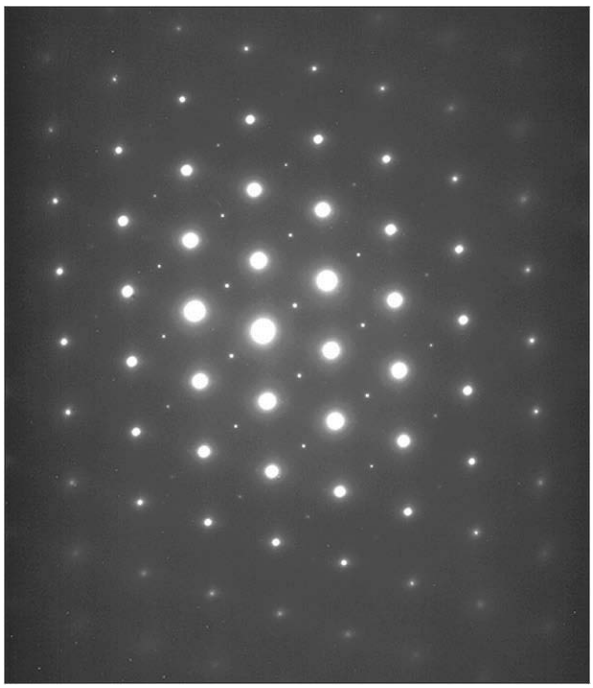

b)

Figure 6 – Dark field transmission electron micrograph a) and corresponding electron diffraction pattern b) for slightly overaged (at 650 °C) DLF alloy K-500

was discussed by Dey *et al.* and five strengthening mechanisms were identified [2]:

- Coherency strain hardening
- Surface hardening
- Order hardening – antiphase boundary (APB) hardening by dislocation cutting
- Stacking fault hardening by dislocation cutting
- Modulus mismatch hardening

The work by Dey *et al.* described the strengthening mechanisms for each, and the major contribution to strengthening in K-500 was assumed to be the cutting of ordered $Ni_3(TiAl)$ precipitates by dislocations and thus the formation of an antiphase boundary, since the lattice misfit between the $Ni_3(TiAl)$ precipitate and the FCC matrix was determined to be small [2].

Based upon the observations of Dey *et al.* [2] and following the methodology of Nembach and Neite [4], which

combine the models of Brown and Ham [5] and Haasan and Labusch [6], the change in flow stress, $\Delta\tau$, can be shown to have the following relationship when weakly coupled dislocation pairs are cutting coherent ordered precipitates:

$$\Delta\tau = \frac{\gamma_{APB}}{2b}\left[A_1\left(\frac{\gamma_{APB}rf}{T}\right)^{\frac{1}{2}} + A_2 f\right] \quad (1)$$

where

A_1, A_2 -Constants (0.91 and -0.55, respectively)

b - Burgers Vector

r - Average Precipitate Radius

f - Volume Fraction of Precipitate

T - Line Tension of Dislocation

γ_{APB} - Anti-Phase Boundary Energy

The second term can be shown to decrease the strength by less than approximately 7 percent, so that Equation 1 can now be written as:

$$\Delta\tau \cong \frac{\gamma_{APB}A_1}{2b}\left(\frac{\gamma_{APB}rf}{T}\right)^{\frac{1}{2}} \propto (rf)^{\frac{1}{2}} \quad (2)$$

Based upon the observed lack of incubation period, the assumption of site saturation (*i.e.,* zero nucleation rate) was made. For site saturation, the volume fraction of spherical precipitates is related to the radius of the precipitates as follows:

$$f \propto r^3 \quad (3)$$

Substituting Equation 3 into Equation 2, the change in flow stress is now taken to be related to the volume fraction of precipitate as follows:

$$\Delta\tau \propto f^{2/3} \quad (4)$$

From Inco alloy data [7], it was found that the Rockwell B hardness was found to be related to 0.2% offset yield stress as follows (from the curve-fit of the data):

$$HR_B \propto \sigma^{0.3}_{0.2\%Y.S.} \text{ and } \Delta HR_B \propto \Delta\sigma^{0.44}_{0.2\%Y.S.} \quad (5)$$

Taking the change in flow stress to be directly proportional to the change in 0.2% offset yield stress, it can be seen that the change in hardness is related to the change in flow stress (and thus volume fraction precipitate) in a simplified form:

$$\Delta HR_B \propto \Delta\tau^{0.44} \propto (f^{2/3})^{0.44} \quad (6)$$

It has been shown in various precipitation-strenghtened materials that the overall precipitation kinetics follows the form of the Johnson-Mehl-Avrami (JMA) equation [8-12]:

$$x = [kt]^n \quad (7)$$

where:

x = volume fraction transformed

t = time

k =rate constant

n = time exponent (typically independent of temperature)

However, this form of the JMA equation is not usually applicable to isothermal precipitation reactions, even when the transformation product is less than 10 % of the total volume of material (*e.g.,* precipitation-strengthening reactions). It has been shown by Christian [12] that for these types of reactions, adjacent diffusional volumes overlap (or impinge) during the reaction (except at early stages in the reaction), and the concept of soft impingement or impingement of diffusional volumes is now treated by using the impinged volume form of the JMA Equations [8-12]:

$$x = 1 - \exp(-kt)^n \quad (8)$$

The time exponent, n, may be useful in understanding the nature of the isothermal reaction by predicting reaction conditions and morphologies of the reaction product, provided that the reaction conditions and morphologies remain similar throughout the isothermal kinetic window investigated. Table 3 shows a list of expected n-values for a number of reactions [12]. It should be stated that this list is by no means exhaustive, but it does provide a reasonably complete list of expected reaction conditions/morphologies for most metallurgical processes. Experimental n-values are easily determined by rearranging Equation 8 to provide a plot of the log log (1/(1-x)) *vs* log t. The result of a plot such as this is linear with n as the slope. In previous investigations, the volume fraction of precipitate has been related to a measured property such as resistivity or hardness.

Taking the volume fraction of precipitate to be linearly related to the volume fraction transformed, the hardness is shown to be related to the volume fraction transformed as follows:

$$f \propto x \propto \Delta HR_B^{3.3} \quad (9)$$

Finally, to utilize the JMA relationship (to find the n-values), the change in hardness is normalized with respect to the total hardness change (at peak hardness – *i.e.*, prior to overaging). Equation 8 may now be rewritten as

$$\Delta HR_B\,(t)^{3.3} / \Delta HR_B\,(TOT)^{3.3} \propto x = 1 - \exp(-kt)^n \quad (11)$$

The values of log log $1/(1 - (\Delta HR_B\,(t)^{3.3} / \Delta HR_B\,(TOT)^{3.3}))$ are plotted *vs* log t in Figure 7 to obtain n-values for isothermal precipitation in alloy K-500. A similar analysis was performed by Robino *et al.* [13] on a precipitation-hardenable martensitic stainless steel. JMA values are obtained from the slope of the straight lines in this plot. At 600 °C, the n-values were found to vary from between 1.1 and

Table 3 – Predicted n-values for JMA kinetics analyses [12]

Polymorphic Changes, Discontinuous Precipitation, Eutectoid Reactions, Interface Controlled Growth, *etc.*	
Conditions	**N**
Increasing Nucleation Rate	>4
Constant Nucleation Rate	4
Decreasing Nucleation Rate	3-4
Zero Nucleation Rate (Saturation Of Point Sites)	3
Grain Edge Nucleation After Saturation	2
Grain Boundary Nucleation After Saturation	1
Diffusion Controlled Growth	
Conditions	**N**
All Shapes Growing From Small Dimensions, Increasing Nucleation Rate	>2.5
All Shapes Growing From Small Dimensions, Constant Nucleation Rate	2.5
All Shapes Growing From Small Dimensions, Decreasing Nucleation Rate	1.5-2.5
All Shapes Growing From Small Dimensions, Zero Nucleation Rate	1.5
Growth Of Particles Of Appreciable Initial Volume	1-1.5
Needles And Plates Of Finite Long Dimensions, Small In Comparison With Their Separation	1
Thickening Of Long Cylinders (Needles) (e.g. After Complete Edge Impingement)	1
Thickening Of Very Large Plates(e.g. After Complete Edge Impingement)	0.5
Precipitation On Dislocations (Very Early Stages)	~0.667

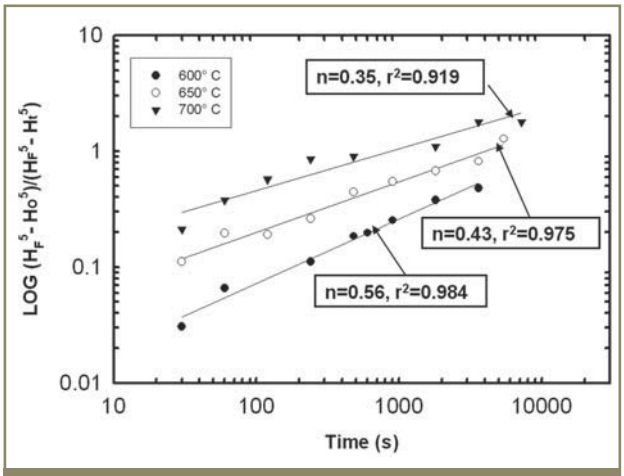

Figure 7 – Plot of log $(HR_{BF}^{5} - HR_{B0}^{5}) / (HR_{BF}^{5} - HR_{Bi}^{5})$ *versus* time for laser-deposited alloy K-500. Note the low n-value from the JMA analysis indicating a rapid precipitation behavior

1.3. Based upon the predicted values from Table 3, these n-values predict that the nucleation and growth mechanism is "growth of particles of appreciable initial volume" [12]. This is interpreted as meaning that nucleation and some growth has already occurred prior to the aging of the precipitates. At 650 °C, the n-values were found to vary from 0.77 to 0.96, and at 600 °C, the n-values were found to vary from 0.6 to 0.66. This analysis determined that as the aging temperature increased, the n-values were found to decrease, suggesting a mechanism change for hardneing with changing temperature.

Usually, the isothermal transformation kinetics are coupled with Arrhenius-type plots (to obtain the apparent activation energy of the process) to verify the kinetic analysis results. However, since only three aging temperatures were investigated and the mechanisim for precipitation hardening appears to be changing, an Arrhenius-type analysis is not useful.

Others such as Herman and Fine [14] and Ballufi and Seidman [15] have shown that the kinetics of aging and annealing are influenced by the decay of quenched-in vacancies. The kinetics of the decay of quenched-in vacancies have been described by n-values of 2/3. This decay was believed to contribute to a more rapid precipitation in an Al-6Ag alloy [14]. Given the observations and analysis in the present study, it is likely that a number of factors may influence the kinetics of precipitation in alloy K-500 as the temperature is increased. The observation of superlattice reflections in the as-deposited material indicates that zero nucleation rate is feasible, and that the growth of the precipitates of apprciable initial volume is also feasible, as predicted with the lowest aging temperature. At elevated temperatures, precipitation hardening of K-500 is most likely occuring with competing mechanisms, such as the decay of quenched-in vacancies or a sizable fraction of precipitates along the grain boundaries with even fewer precipitates along the dislocations. Other interpretations of n-values less than unity include (1) growth of precipitates of appreciable initial volume and (2) simultaneous growth and coarsening.

5 Implications

It was found in the current investigation that the precipitation kinetics of the DLF and heat treated K-500 are similar to the wrought and heat treated K-500, as illustrated in the summary plot of the change in hardness and time to peak hardness (Figure 8). Similar behavior is anticipated for laser welded K-500. Thus, the welded K-500 material may be heat treated in a similar manner to the wrought material, and the resulting hardness should be similar.

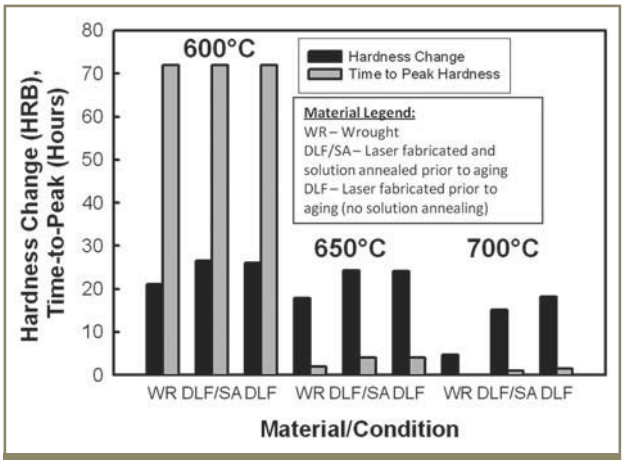

Figure 8 – Summary plot showing the change in hardness and time to peak hardness as it applies to the material condition

6 Conclusions

Several conclusions can be made regarding the heat treatment response of alloy K-500 in the DLF (or laser-welded) condition. These include:

1. The heat treatment of DLF K-500 is similar to its wrought counterpart, suggesting that post-weld heat treatments of K-500 should respond in a similar fashion to the wrought material.
2. The isothermal transformation kinetics of the gamma-prime $Ni_3(TiAl)$ precipitate exhibit a change in hardening response as a function of temperature.
3. At 600 °C, the kinetics analysis determined that the n-values varied from 1.1 to 1.3, suggesting growth of precipitates of appreciable initial volume. The n-values were found to be less than unity for aging at higher temperatures, with the n-values decreasing as temperatures increased. This suggests that the mechanism for precipitation hardening was changing as the temperature was increased. This suggests that a process such the decay of quenched-in vacancies, precipitation along the grain boundaries, or precipitation along the dislocations (or a combination of any of these) aids in the rapid precipitation.

Acknowledgements

This work was performed at Los Alamos National Laboratory, an affirmative action/equal opportunity employer, operated by the Los Alamos National Security, LLC for the National Nuclear Security Administration of the U.S. Department of Energy under contract DE-AC52-06NA25396.

References

[1] Dey G.K. and Mukhopadhyay P.: Precipitation in the Ni-Cu-base Alloy Monel K-500, Materials Science and Engineering, 1986, vol. 84, issue 1-2, pp. 177-89.

[2] Dey G.K., Tewari R., Rao P., Wadekar S.L. and Mukhopadhyay P.: Precipitation Hardening in Nickel-Copper Base Alloy Monel K 500, Metall. Trans A, 1993, vol. 24A, no. 12, pp. 2709-19.

[3] Hochanadel P.W., Lienert T.J., Martinez J.N., Martinez R.J. and Johnson M.Q.: Weld Solidification Cracking in 304 to 304L Stainless Steel, Hot Cracking Phenomenon in Welds III, J. Lippold, T. Böllinghaus and C. Cross, eds., Springer-Verlag, Berlin Heidelberg, 2011, pp. 145-160.

[4] Nembach E. and Niete G.: Precipitation Hardening of Superalloys by Ordered γ'-Particles, Prog. Materials Science, 1985, vol. 29, issue 3, pp. 177-319.

[5] Brown L.M. and Ham R.K.: Chapter 2 – Dislocation-Particle Interactions, Strengthening Methods in Crystals, A. Kelly and R.B. Nicholson, eds., John Wiley and Sons, New York, NY, 1971, pp. 9-135.

[6] Haasen P. and R. Labusch: Precipitation Hardening by Large Volume Fractions of Ordered Particles, Proc. 5th International Conference on the Strength of Metals and Alloys, Haasen P., Gerold V. and Kostorz G., eds., Pergamon Press, Toronto, 1979, vol. 1, p. 639-44.

[7] Monel® Nickel-Copper Alloys, Publication No. IAI-170, Inco Alloys International, Huntington, WV, Fifth Ed., 1984, p. 6.

[8] Avrami M.: Kinetics of Phase Change I – General Theory, J. Chem. Phys., 1939, vol. 7, issue 12, pp. 1103-12.

[9] Avrami M.: Kinetics of Phase Change II – Transformation-Time Relations for Random Distribution of Nuclei, J. Chem. Phys., 1940, vol. 8, issue 2, pp. 212-24.

[10] Avrami M.: Kinetics of Phase Change III – Granulation, Phase Change and Microstructure", J. Chem. Phys., 1941, vol. 9, issue 2, pp. 177-84.

[11] Johnson W.A. and Mehl K.E.: Reaction Kinetics in Processes of Nucleation and Growth, Trans. AIME, 1939, vol. 195, issue 8, pp. 416-42.

[12] Christian J.W.: The Theory of Phase Transformations in Metals and Alloys, Part I, Pergamon Press, New York, NY, 1981, p. 542.

[13] Robino C.V., Hochanadel P.W., Edwards G.R. and Cieslak M.J.: Heat Treatment of Investment Cast PH-13-8 Mo Stainless Steel: Part II. Isothermal Aging Kinetics, Metall. Trans. A, 1994, vol. 25A, issue 4, pp. 697-704.

[14] Herman H. and Fine M.E.: An Accoustical Study of Low-Temperature Age-Hardening after Reversion in Al-6 At. Pct Ag, Trans. Met. Soc. AIME, 1960, vol. 218, issue 1, pp. 44-9.

[15] Ballufi R.W. and Seidman D.N.: Annealing Kinetics of Vacancies to Dislocations, Phil. Mag., 1968, vol. 17, issue 148, pp. 843-8.

About the authors

P.W. Hochanadel, R.D. Field and G.K. Lewis are with the Los Alamos National Laboratory, Los Alamos (USA).